Author Manuscript

Author Manuscript

Author Manuscript

Author Manuscript

HHS Public Access

Author manuscript

Biomaterials. Author manuscript; available in PMC 2020 December 01.

Published in final edited form as:

Biomaterials. 2019 December ; 225: 119519. doi:10.1016/j.biomaterials.2019.119519.

Zwitterionic polymer/ polydopamine coating reduce acute inflammatory tissue responses to neural implants

Asiyeh Golabchi[1,2], **Bingchen Wu**[1,2], **Bin Cao**[1,2], **Christopher J. Bettinger**[3,4], **Xinyan Tracy Cui**[1,2,4,*]

[1]Department of Bioengineering, University of Pittsburgh.

[2]Center for Neural Basis of Cognition.

[3]Department of Biomedical Engineering, Department of Material Science and Engineering, Carnegie Mellon University.

[4]McGowan Institute for Regenerative Medicine, University of Pittsburgh.

Abstract

The inflammatory brain tissue response to implanted neural electrode devices has hindered the longevity of these implants. Zwitterionic polymers have a potent anti-fouling effect that decreases the foreign body response to subcutaneous implants. In this study, we developed a nanoscale anti-fouling coating composed of zwitterionic poly (sulfobetaine methacrylate) (PSB) and polydopamine (PDA) for neural probes. The addition of PDA improved the stability of the coating compared to PSB alone, without compromising the anti-fouling properties of the film. PDA-PSB coating reduced protein adsorption by 89% compared to bare Si samples, while fibroblast adhesion was reduced by 86%. PDA-PSB coated silicon based neural probes were implanted into mouse brain, and the inflammatory tissue responses to the implants were assessed by immunohistochemistry one week after implantation. The PSB-PDA coated implants showed a significantly decreased expression of glial fibrillary acidic protein (GFAP), a marker for reactive astrocytes, within 70 μm from the electrode-tissue interface ($p<0.05$). Additionally, the coating reduced the microglia activation as shown in decreased Iba-1 and lectin staining, and improved blood-brain barrier integrity indicated by reduced immunoglobulin (IgG) leakage into the tissue around the probes. These findings demonstrate that anti-fouling zwitterionic coating is effective in suppressing the acute inflammatory brain tissue response to implants, and should be further investigated for its potential to improve chronic performance of neural implants.

*Corresponding author: X. Tracy Cui, Ph.D., Department of Bioengineering, University of Pittsburgh, 5057 Biomedical Science Tower 3, 3501 Fifth Avenue, Pittsburgh, PA 15260, Ph: 412-383-6672, Fx: 412-648-9076, xic11@pitt.edu.

Publisher's Disclaimer: This is a PDF file of an unedited manuscript that has been accepted for publication. As a service to our customers we are providing this early version of the manuscript. The manuscript will undergo copyediting, typesetting, and review of the resulting proof before it is published in its final form. Please note that during the production process errors may be discovered which could affect the content, and all legal disclaimers that apply to the journal pertain.

Competing interests: The authors have no conflict of interest related to this research to disclose.

Data and materials availability: The datasets generated during and/or analyzed during the current study are available from the corresponding author on reasonable request.

Author Manuscript Author Manuscript Author Manuscript Author Manuscript

Keywords

Biocompatibility; Zwitterionic coating; Catechol; Protein adsorption; Inflammatory tissue responses; Gliosis; Neural implants; Poly sulfobetaine methacrylate; Polydopamine

1. Introduction

The application of implantable electrodes as neuroprosthetic devices capable of electrically stimulating neurons and recording neural activities has demonstrated great potential in treating neurological disorders and assisting paralyzed patients via controlling external robotic arms [1–3]. However, neural recording devices experience degradation of signal quality over extended periods of implantation. One major contributing factor to the recording failure is the undesired inflammatory host tissue response to the implanted electrode, leading to acute and chronic microglia activation, neuronal loss and silencing, glial scarring, persistent leakage of the blood brain barrier (BBB), and demyelination [4, 5]. Similar host responses also have been shown to reduce the sensitivity and detection capability of implanted biosensors [4].

During insertion, the microelectrode tears blood vessels, mechanically damages the membrane of neuronal and glial cells, and breaches the BBB [6, 7]. The insertion damage triggers an immediate response from the resident microglia cells which extend their processes to the probe surface and attach and spread in an effort to encapsulate the device [8–10]. The vascular damage releases serum proteins into the surrounding parenchyma. Many of these proteins such as fibrinogen, albumin, and complement proteins are pro-inflammatory and neurotoxic, and when adsorbed onto the electrode material surface, may promote the adhesion and activation of microglia and macrophage on the surface of the device [4]. This triggers a cascade of inflammatory tissue responses. Over time, a scar primarily made of microglia, activated astrocytes, and fibroblasts is formed and acts as a barrier to signal transmission between the electrode and nearby neurons [4, 11]. Moreover, neuronal loss and neurite degeneration is observed which could lead to degradation of recording signals [12, 13].

Because of the critical role that protein adsorption plays in host tissue response, decreasing the adsorption of serum protein onto the implant surface may suppress microglia/macrophage aggregation and activation, which further minimizes the inflammation cascade and neuronal loss. It is documented that biomaterial surface properties can affect the types, concentration, conformation, orientation, and binding strength of the adsorbed proteins [14]. In an attempt to reduce protein adsorption and inflammatory cell attachment, different strategies have been developed through surface coatings and modifications of the implants surface [15–17]. Historically, modifying the hydrophobic surface of implants with hydrophilic materials has been a primary approach due to their low-fouling nature and the consequently improved tissue response [18, 19]. A gold standard hydrophilic material is poly (ethylene glycol) (PEG), which has been widely applied to implantable devices for protein-resistant applications [20–22]. However, PEG hydrogels are susceptible to thermal [23] and slow oxidative degradation *in vivo* [24] and have been shown to cause specific

Author Manuscript Author Manuscript Author Manuscript Author Manuscript

antibody based immune responses [25, 26]. In addition, poly (2-hydroxyethyl methacrylate) (pHEMA) is another low-fouling candidate for *in vitro* [27–29] and *in vivo* applications [30], but pHEMA implants still generate considerable level of fibrotic encapsulation [17]. Therefore, a more robust and biocompatible non-fouling surface modification is necessary.

Recent studies have shown that zwitterionic materials containing phosphorylcholine (PC), carboxybetaine (CB) [31], and sulfobetaine (SB) [32, 33] functional groups are superior to conventional PEG and pHEMA coatings, due to their higher resistance to nonspecific protein adsorption (<0.3 ng cm^{-2}) [34, 35]. The fouling resistance of these zwitterionic materials is based on their strong interactions with water, forming a hydration layer bound through solvation of the charged terminal groups [36]. Zwitterionic PSB grafted membranes exhibited significant reduction in human fibrinogen adsorption (~90%) compared to a control [37]. The Jiang group reported lower fibrinogen adsorption in poly(carboxybetaine methacrylate) (PCBMA) grafted membranes compared to a glass control [33]. They further showed that PCBMA hydrogels implanted subcutaneously in mice for 3 months resist fibrous capsule formation, demonstrating excellent *in vivo* antifouling performance [17]. Despite the progress in the development in zwitterionic surface coating, the effect of zwitterionic coating on neural implants is not known.

One way to graft the zwitterionic polymer on surfaces is by using a biomimetic catechol group which has been shown to strongly attach to most surfaces [38, 39]. Several studies have reported successful grafting of zwitterionic polymers via a catechol anchor group on silica, gold, and iron oxide substrates and have demonstrated ultralow fouling [40–42]. Here, we developed and compared two different coating methods to modify the silicon implant surface with zwitterionic polymer PSB. The first method employs PSB only and utilizes a catechol end group to accomplish the surface grafting. The second method involves co-deposition of PDA and PSB, which demonstrated superior stability *in vitro*. Non-functional single shank silicon probes (NeuroNexus, MI) were coated with PDA-PSB and implanted in the visual cortex of C57BL/6 male mice for 1 week to examine inflammatory response to the implants using quantitative immunohistochemistry.

2. Materials and Methods

2.1. Preparation of zwitterionic coating

2.1.1. Materials—Copper(I) Bromide (CuBr 98%), imidazole (≥99%), bromoisobutyryl bromide (BIBB 98%), [2-(methacryloyloxy)ethyl]-dimethyl-(3-sulfopropyl) ammonium hydroxide (SBMA 97%), 2,2’-bipyridine (BPY, ≥99%), Tetrahydrofluran (THF), Tert-butyl chlorodimethylsilane (TBDMS, 97%), Triethylamine(TEA) were purchased from Sigma-Aldrich. Tetrabutylammonium fluoride (TBAF), and Dopamine-HCl (99%) were purchased from ACROS.

2-[3, 4-Di (t-butyldimethylsilyloxy)] phenethylamine (1 in Scheme 1): As shown in the step 1 of Scheme 1, using a similar method reported previously [40], the catechol oxygens were protected by reacting dopamine-HCl with TBDMS. Compound 1 was obtained and purified after the reaction. In brief, Dopamine-HCl (2.72 g, 14.3 mmol) and imidazole (4.3 g, 71 mmol) were dissolved in dry THF (50 ml) and added into a round bottom flask under

Author Manuscript Author Manuscript Author Manuscript Author Manuscript

N_2 purge. Then TBDMS (6.48 g, 43 mmol) was dissolved in dry THF and slowly added into the flask. The reaction was carried out at room temperature for 3 hours. After filtration of the precipitate, removal of solvent, final mixture was purified by silica gel chromatography with dichloromethane-methanol (4:1). Both ^{1}H and ^{13}C NMR spectra can be found in supplemental material (Fig. S. 1. & Fig. S. 2). ^{1}H NMR (400Hz, $CDCl_3$), δ [ppm]: 6.75–6.71 (m, 3H), 3.19–3.15 (q, J=8Hz, 2H), 2.98–2.94 (q, J=8Hz, 2H), 1.26 (s, 2H), 0.98 (s, 18H), 0.18 (s, 12H). ^{13}C, NMR, δ [ppm]: 171.99, 147.04, 145.78, 131.67, 121.87, 121.73, 121.30, 41.66, 33.85, 30.2, 25.90, −3.86.

2-Bromo-2-methyl-N-[2-(3, 4-di (t-butyldimethylsilyloxy)-phenyl)-ethyl] propionamide (2 in Scheme 1): As shown in the step 2 of Scheme 1, compound 2 was obtained by reacting 1 with BIBB following a method previously reported [40]. In brief, compound 1 (6 g, 14.3 mmol) was dissolved in dry THF and transferred into a flask under N_2 purge. Then TEA (2.2 ml, 15.8 mmol) was mixed with 20 ml of THF and added into the flask. The mixture was cooled to 0°C using an ice bath, then BIBB (3.95 g, 17.16 mmol) was mixed with 15 ml of THF and added into the flask. The reaction was carried out at room temperature overnight. After filtration of the precipitate and removal of solvent, the crude product was dissolved in ether, washed with $NaHCO_3$ solution 3 times, dried with $MgSO_4$, and passed through a silica gel chromatography with hexane-ethyl acetate (2:1). Pure product was collected after filtration and vacuum drying as white crystal. Both ^{1}H and ^{13}C NMR spectra of can be found in supplemental material (Fig. S. 3 & Fig. S. 4). ^{1}H NMR (400Hz, $CDCl_3$), δ [ppm]: 6.71–6.63 (m, 3H), 3.49–3.44 (q, J=8Hz, 2H), 2.73–2.70 (t, J=8Hz, 2H), 1.90 (s, 2H), 0.98–0.97 (d, J=4Hz, 18H), 0.19–0.18 (d, J=4Hz, 12H). ^{13}C, NMR, δ [ppm]: 147.17, 146.25, 129.52, 121.82, 121.74, 121.52, 63.28, 41.71, 34.77, 32.73, 25.86, −3.88.

2.1.2. Synthetize of PSB—The polymerization of SBMA is carried out using a similar method previously reported [40], as shown in Scheme 2. In brief, compound 2 (106 mg, 0.2 mmol), SBMA (1.12 g, 4 mmol) were mixed in flask A, removed of O_2 by filling N_2. BPY (62.4 mg, 0.4 mmol), and CuBr (28.6 mg, 0.2 mmol) were mixed in flask B and removed of O_2 by filling N_2. Both mixtures were dissolved with a solution of water and methanol (4:1, v/v) separately, then mixed together, heated up to 30°, and reacted for 24 hrs with stirring. The product was mixed with 1 mmol TBAF in THF to completely remove TBDMS group before surface adhesion. The average molecular weight (MW) of PSB is measured to be 2.7 $\times 10^5$ g/mol using Agilent 1000 Series with a SEC column (YMC-Pack Diol-300 S-5um, 30mm 300×6.0 mm). The experiment was carried out in 50 mM TRIS (pH 8.0) buffer under1 mL/min flow rate with a 100 μl injection volume. PSB, 2 mg/mL was dissolved in 10 mM TRIS buffer. The system was calibrated with Bio-Rad 151–1901 standard.

2.2. Characterization

2.2.1. *In vitro* surface coating stability assessment (thickness and contact angle)—Silicon wafers were used as substrates for *in vitro* stability tests. Before polymer grafting, substrates were sonicated for 5 mins in acetone, isopropanol, and Millipore water sequentially and dried under N_2 flow. Two different polymer grafting methods were used to modify the substrate surface (Scheme 3). Method 1 is dip-coating using PSB only. The substrates were immersed in Tris buffer (10 mM) solution of PSB (2 mg/ml) for 24 hrs.

Author Manuscript Author Manuscript Author Manuscript Author Manuscript

Method 2 combined PSB with PDA to form a co-deposition of PDA and PSB (PDA-PSB) polymer film. The substrates were immersed in a Tris buffer (10 mM) solution of PSBMA-catechol (2 mg/ml) and dopamine (1 mg/ml) for 24 hrs. Post surface modification, all samples were rinsed with DI-water and dried under N_2 flow. The thickness of the polymer film was measured using an ellipsometer (J. A. Woollam α-SE) and data was fitted with a Cauchy Model using refractive index of 1.45 and water contact angles were measured using AST Products VCA Optima. Then all samples were immersed in PBS solution for 4 weeks. At week 1, week 2, and week 4, samples were rinsed with DI-water, dried under N_2 flow, and subjected to ellipsometry and water contact angle measurements. For ellipsometry, n=8 before soaking and 1 week of soaking, and n=6 at 2 and 4 weeks of soaking. For measuring water contact angle, n=12 for PDA films, n=6 for PSB films, and n= 4 (before and 1 week after soaking, n=6 for 2 and 4 weeks of soaking for PDA-PSB films.

2.2.3. X-ray Photoelectron Spectroscopy (XPS) analysis—XPS measurements were performed using Surface Science Instruments X-Probe spectrometers to investigate the surface composition of the PSB and PDA-PSB films. The ESCALAB 250Xi XPS spectrometer microprobe (Thermo Fisher Scientific, MA, USA) with an Al Kα X-ray source (1486.71 eV of photons) was used. The pressure in the analysis chamber was maintained at about 8×10^{-7} Pa during each measurement. The survey spectra (from 0 to1400 eV) and the core-level spectra with higher resolution were both collected. An ion gun was used to compensate for surface charge effects. The software Thermo scientific™ Avantage Data system was used to fit the XPS spectra peaks.

2.2.4. *In vitro* anti-fouling performance assessment (protein adsorption and cell adhesion)—All samplers were rinsed with DI-water, dried under N_2 flow. The thickness of polymer films was determined using ellipsometer, and then soaked in fibrinogen (1 mg/ml) PBS solution for 30 mins. Post soaking thicknesses were measured and the initial polymer thickness was subtracted from the measurement to get an estimate of the protein absorption. Bare silicon wafers were used as control group. For fibroblast attachment assay, all samples were sterilized under UV for 20 mins before culturing 3T3 fibroblast cells. A cell density of 25 k/cm^2 was used to plate the fibroblasts. All samples were incubated for 24 hrs at 37°C, then fixed with 4% paraformaldehyde, stained, and subjected to fluorescence imaging. The number of samples for protein adsorption test and cell attachment test was 6 and 8 for each group, respectively. Further, to evaluate the protein adsorption behavior on the bare and PDA-PSB coated probes, the plasma protein IgG (2 g/ml) and albumin protein (2 mg/mL) were used. Probes were immersed in each protein solution for 1 hour and followed with PBS wash. Then, the fluorescence images were taken using Leica DFC350 FX microscope.

2.3. Surface coating of neural electrodes with a PDA-PSB

Non-functional single shank NeuroNexus electrodes (A1X16–3MM-100–703-CM15) were first gently rinsed with acetone and isopropanol 3 times in sequence and air dried. Then probes were rinsed with PBS 3 times prior to coating process. The probes were then immersed in a Tris buffer (10 mM) solution of PSB (2 mg/ml) and dopamine (1 mg/ml) for

Author Manuscript Author Manuscript Author Manuscript Author Manuscript

24 hrs. Post surface modification, probes were gently rinsed with PBS 3 times and sterilized with ethylene oxide before surgery.

2.4. Surgical procedure for *in vivo* biocompatibility in rodent brain

C57BL/6J 9–12-week-old male mice were purchased form The Jackson Lab., Bar Harbor, ME and were kept with a 12:12-h light: dark cycle and with ad libitum access to the food and water in the temperature-controlled animal facility center. All procedures followed NIH and federal guidelines and were approved by the University of Pittsburgh, Institutional Animal Care & Use Committee.

Mice were anesthetized by using an Isoflurane Vaporizer (Patterson Veterinary Inc.; isoflurane inflow was 2% for induction phase and maintained at 1.5% during surgery) that provides a mixture of isoflurane and oxygen. A warm water pad (HTP 1500, Adroit Medical Systems, Loudon, TN) was set to 37 °C and placed underneath the anesthetized mouse to maintain body temperature. The mouse was mounted to the stereotaxic frame (Kopf Instruments, Tujunga, CA) and the skull was exposed. The hole was drilled in the skull with a surgical drill (0.007 drill bit, Fine Science Tools, Inc., Foster City, CA) measuring 1 mm anterior to Lambda and 1.5 mm lateral to midline. Sterilized saline was applied continuously for cutting heat dissipation in high-speed drilling of bone. Three sterilized bone screw (Stainless Steel; shaft diameter: 1.17 mm, length: 4.7 mm; Fine Science Tools, Inc., Foster City, CA) were screwed bilaterally over the primary motor cortex and over the contralateral visual cortex for anchoring dental cement to bone. The coated (PDA-PSB) or non-coated (control) probes were implanted into the left visual cortex of mice using a stereotaxic vacuum manipulator until the top edge of the last electrode site was at the surface of the brain. Each mouse was implanted with one electrode and 4 mice were implanted for each condition. After filling the craniotomy with Kwik-Cast Sealant (World Precision Instruments, Sarasota, FL), dental cement (Pentron Clinical, Orange CA) was cured with a dental curing light to make a head-cap. After surgery, animals received intraperitoneal (i.p.) injection of 5 mg/kg ketofen (100 mg/ml, Zoetis Inc, Kalamazoo, MI) and placed on an electric heating blanket under a warming light to wake up. During the first three days after surgery, daily use of analgesic was administered.

2.5. Immunohistochemistry

After one week, mice were sacrificed and deeply anesthetized using 80–100 mg/kg ketamine, 5–10 mg/kg xylazine cocktail. Once mice were unresponsive to tail/toe pinches, animals were transcardially perfused using phosphate buffered saline (PBS) flush at <80 mmHg followed by 4% paraformaldehyde (PFA) at <80 mmHg. Mice were decapitated and the skulls were partially removed to post-fix the brain in a 4% PFA at 4 °C for 4–6 h. Following electrode retrieval, brains were stored immediately in 4% PFA overnight and the day after soaked in a 15% sucrose (Sigma-Aldrich Corp., St. Louis, Missouri) bath at 4 °C overnight followed by a 30% sucrose solution for 24 h. Brains were then carefully frozen in a 2:1 20% sucrose in PBS:optimal cutting temperature compound (Tissue-Plus O.C.T. Compound, Fisher HealthCare, Houston, TX) blocking media blend with dry ice. Frozen tissue was then horizontally sectioned into 25 m thick sections along the tract of the probes using a cryostat (Leica CM1950, Buffalo Grove, IL).

Author Manuscript Author Manuscript Author Manuscript Author Manuscript

Cortical sections of implanted and non-implanted hemisphere were mounted on the same slide for comparison and histological staining for each antibody combination was performed at the same time to minimize variability. The inflammatory response after 1 week were examined using NeuN (neurons, 1:250, MAB377 Millipore), NF200 (mature axons, 1:250, MAB5256 Millipore), IBA-1(microglia, 1:500, NC9288364 Fisher), GFAP (astrocytes, 1:500, Z033401 Dako), and IgG (blood-brain barrier injury, 1:16, Alexa Flour 647-conjugated AffiniPure Fab Fragment goat anti-mouse IgG 115-607-003 Jackson ImmunoResearch Laboratories, Inc.). These antibodies were used to investigate the effect of zwitterionic coating in glial activation and probe encapsulation. Besides, biotinylated lycopersicon esculentum, tomato lectin (1:250, B1175 Vector Labs) was used to label blood vessels and microglial cells.

Tissue sections were rehydrated in 1x PBS for 2×5 min. The tissues were then incubated in 0.01 M sodium citrate buffer for 30 min at 60 ° C. Then, a peroxidase block (PBS with 10% v/v methanol and 3% v/v hydrogen peroxide) was performed for 20 min at room temperature (RT) on a table shaker. Next, tissue section were incubated in carrier solution (1 X PBS, 5% normal goat serum, 0.1% Triton X-100) for 30 min at RT. Lastly, the tissue sections were blocked with Alexa Flour 647-conjugated AffiniPure Fab Fragment goat anti-mouse IgG (IgG, 1:16, 115-607-003 Jackson ImmunoResearch Laboratories, Inc.) or Fab fragment only (1:13, 115-007-003, JacksonImmunoResearch Laboratories, Inc.) for 2 hrs then rinsed 6 times each 4 minutes. Following blocking, sections incubated in a primary antibody solution consisting of carrier solution and antibodies listed before overnight (12–18 hrs) at RT Sections were then washed with 1x PBS for 3X5 min and incubated in carrier solution and secondary antibodies (1:500, Alexa Flour 488 goat-anti mouse, Invitrogen, and 1:500 Alexa Flour 568 goat-anti rabbit, Invitrogen, 1:500, DyLight 649 Streptavidin, Vector Labs, 1:500 Alexa Flour 568 goat-anti mouse, Invitrogen, 1:500 Alexa Flour 488 goat-anti rabbit, Invitrogen, 1:500 Alexa Flour 633 goat-anti chicken, Invitrogen) for 2 hrs at RT. Then sections were rinsed with PBS for 3×5 min and exposed to Hoechst (1:1000, 33342 Invitrogen) for 10 min and washed in PBS for 3×5 min before being cover slipped with Fluoromount-G (Southern Biotech, Associate Birmingham, AL).

2.6. Imaging and quantitative tissue analysis

All images were acquired on Olympus Fluoview 1000 II Confocal Microscope (Olympus America, Center Valley, PA) at the Center for Biologic Imaging at the University of Pittsburgh to examine the cellular reactions associated with the implanted electrodes. For each antibody, images were taken using the same laser power, exposure time, and detector settings to decrease variability. Images were centered on the implant site and multi-channel images were acquired simultaneously. For GFAP, tomato lectin, Iba-1, and IgG images were analyzed using a pixel-based radial image intensity analysis as previously described [43, 44]. Sections in the range of 500 μm to 1000 μm depth from brain surface were compared with control (non-implanted) section. For each image, the center of insertion site was chosen and by using MATLAB script, masks of concentric rings every 20 μm for 240 μm was generated. Then, MATLAB scrip calculated and normalized the average gray scale intensity for all pixels above the threshold of the background noise intensity in each 20 μm bin. Finally, intensities were averaged for each group (control, PDA-PSB), and then bar graphs for

Author Manuscript Author Manuscript Author Manuscript Author Manuscript

intensity-based radial analysis of fluorescent markers were plotted by mean ± standard error as a function of distance.

For NeuN staining, cells were manually counted in each bin and cell density (cell count per tissue area) was calculated. As previously, data were averaged for each group, and the bar graphs for density-based radial analysis of cells (the mean and standard error) were plotted as a function of distance to the implantation site.

2.7. Explanted probes

Additional 2 animals were implanted with 2 coated and 2 control on each side of the hemisphere (n=4 implants for each condition) for explant analysis. One week post implant, the animals were perfused, and decapitated. After post-fixing the head in 4% PFA at 4 C for 6 hours, electrodes were carefully removed and transferred to 4%PFA for 1 hour and stored in PBS for immunohistochemical staining. In addition, coating integrity of the explanted probes was evaluated using scanning electron microscopy (SEM). Following probe extraction, electrodes were fixed using osmium tetroxide (1:10) in DI water solution. Then, probes were rinsed with DI water and dried in ethanol grading from 30% up to 100%. After alcohol vaporization, probes were immersed in hexamethyldisilazane (HMDS) for three hours. Then, air dried over night before imaging with JSM 6335F SEM (JEDOL USA Inc., Peabody, MA, USA). All imaging were conducted at The University of Pittsburgh's Center for Biological Imaging.

2.8. Statistical analysis

Observed experimental differences were assessed for statistical significance through one-way ANOVA (Figure 1 and Figure 2) or two-way ANOVA (Figure 3, Figure 4, Figure 5, and Figure 6) using SPSS. Tukey's post hoc tests were used for all statistical analysis to compare marker expression between groups at different distance from the electrode tissue interface. $p<0.05$ was considered statistically significant.

3. Results

3.2. Synthesis and characterization of the surface coating with PDA-PSB coating

3.2.3. Surface properties and stability of the coating—In this work, we examined two different grafting methods for polymer deposition and compared the anti-fouling properties and the stability of the polymer films. As shown in Figure 1 A, PSB had a water contact angle of 23.3 ± 3.5, and PDA-PSB had a water contact angle of 28.8±3.9 slightly higher than PSB (p=0.008), but significantly lower than PDA (32.7 ± 1.56) (p=0.02). This data suggest that the PDA is more hydrophobic than PSB, and the slight increase in contact angle of PDA-PSB compared to the PSB group indicates that PDA is incorporated in the film and resulting in slightly decreased hydrophilicity. To characterize the polymer composition of PSB and PDA-PSB, XPS analysis was performed. For the PSB coating, C 1s, O 1s, N 1s, S 2p, and Si2p peaks were observed at 285.43 eV, 532.23 eV, 402.69 eV, 167.66 eV, and 99.82eV, respectively (Fig. S. 5). The elemental analysis revealed the atomic ratio of C1s, O1s, N1s, S2p, Si2p being 48.9072%, 22.8616%, 4.8801%, 7.4152%, 15.9359%, respectively. The two peaks near S2p and Si2p satellite peaks and cannot be

Author Manuscript Author Manuscript Author Manuscript Author Manuscript

assigned to any elements. For the PDA-PSB coating, C 1s, O 1s, N 1s S 2p, and Si 2p peaks were observed at 285.42 eV, 531.88 eV, 401.65 eV, 167.71 eV, and 98.93 eV, respectively (Figure 1 B), and the atomic fractions of carbon, oxygen, nitrogen, sulfur and silicon are 25.0181%, 64.2432%, 6.0337%, 3.4664% and 1.2387%, respectively. Based on the elemental ratio of nitrogen to sulfur of PDA-PSB (1.74), the theoretical ratio of PDA to PSB in the PDAPSB coating was calculate to be approximately 1:3.

The finding showed that the thickness of the PSB polymer film significantly decreased after one week of soaking in PBS solution (Figure 1 C; $p<0.001$), and continued to decrease over 4 weeks of study. Before soaking, PSB film thickness was 3.87 ± 0.3 nm (mean±SD), and it decreased to 1.67 ± 0.37 nm, 1.62 ± 0.26 nm, and 1.14 ± 0.28 nm after 1, 2, and 4 weeks of soaking, respectively. On the other hand, the PDA-PSB co-deposition method showed enhanced stability compared to PSB. PDA-PSB thickness was 3.34 ± 1.94 nm before soaking, 2.56 ± 0.96 nm, 3.20 ± 0.59 nm, and 2.86 ± 0.74 nm at 1, 2, and 4 weeks after soaking in PBS, respectively. No significant decrease in the film thickness was observed ($p>0.05$), which indicates that PDA-PSB method can deposit a more stable polymer film compared to PSB film.

Further, the water contact angle confirmed this observation. There was a significant increase in water contact angle of PSB group at week 4 compared to the previous weeks (week 1 and 2) and before soaking (Figure 1 D), which indicated a decrease in hydrophilicity as polymer film worn off. The water contact angle in PSB group remained steady for week 1 (22.6 ± 2.3; mean±SD) and week 2 (23.8 ± 4.9), but increased to 32.4 ± 5.5 at week 4 of soaking in PBS. On the other hand, the PDA-PSB group showed stable water contact angle through the whole experiment time window, with 30.5 ± 3.2 (week-one), 29.3 ± 6 (week-two), and 30.5 ± 6 (week-four) after soaking in PBS ($p>0.05$).

3.2.4. Protein adsorption and cell adhesion assessment—Both protein adsorption and cell attachment assay showed anti-fouling effects from zwitterionic polymer coating. A significantly decreased amount of protein absorption was observed on both PSB and PSB-PDA coated surface comparing to the bare Si wafer (Figure 2 A, $p<0.001$). The thickness of the adsorbed protein layer was 5.22 ± 0.42 nm (mean±SD) on bare Si wafer, while it was 0.03 ± 1.02 nm on PSB coated wafer and 0.53 ± 0.93 nm on PDA-PSB coated wafers. No significant difference in protein adsorption was observed between PSB and PSB-PDA coated substrate ($p>0.05$). Furthermore, we performed the cell attachment test *in vitro* using 3TS fibroblast cells. As shown in Figure 2 (B and C), we observed less cell attachment in both PSB and PDA-PSB coated wafers compared to the bare wafer. Also, a quantitative analysis showed a significantly decreased amount of cell attachment on both PSB and PSB-PDA coated substrate compared to the bare substrate (Figure 2 B). The cell density on Si wafer was approximately 260 ± 83/mm^2 (mean±SD). However, cell numbers decreased to 39 ± 12/mm^2 on PSB coated wafers and to 37 ± 26/mm^2 on PDA-PSB coated surfaces. Moreover, fluorescent tagged proteins, albumin and IgG, were used to evaluate the anti-protein fouling property of the bare and PDA-PSB coated probes. Albumin is one of the most abundant plasma protein in the blood (3.5–5 g/dl) and it is known to cause neurotoxicity/inflammation [45]. IgG (plasma concentration 0.7–1.6g/dl) has been found at the vicinity of the neural implant in immunohistochemical studies and has been used as

Author Manuscript Author Manuscript Author Manuscript Author Manuscript

marker for BBB leakage [46]. As shown in the supplementary data, the amounts of IgG (Fig. S. 6) and albumin (Fig. S. 7) adsorbed on PDA-PSB coated probe were less than those on the uncoated implants based on the fluorescence intensity. Furthermore, the uniform reduction of fluorescence throughout the probe length demonstrates that the PDA-PSB coating was uniformly adherent on the probe surface and effectively resisted protein fouling along the entire shank.

3.2.5. *In vivo* tissue response evaluation—To evaluate the biocompatibility of the PDA-PSB coating after implantation, two groups of implants with and without PDA-PSB coating were implanted into the mice cortex for 1 week and the tissue responses to the implants were assessed through the expression level of GFAP, Iba-1, lectin, IgG, and NF200.

3.2.5.1. Neuronal density and health around the implants: NF200 and NeuN are markers for axons and neuronal cell bodies respectively. The distribution of NF200 as a function of distance for PDA-PSB coated probes presented a similar pattern to the uncoated probes (Figure 3 A and B). The quantified intensity of NF200 as a function of distance to the electrode-tissue interface between the uncoated and PDA-PSB coated was not statistically different (Figure 3 C). Similar to NF200, the distribution of neuronal cells around the device-brain interface was similar in both groups (Figure 3 D and E) and the quantification of neuronal cell density over different distances showed no statistically significant difference for all the bins examined between the coated and uncoated implants (Figure 3 F).

3.2.5.2. Microglia/macrophages reaction in the vicinity of the implants: To evaluate the distribution of microglia or macrophages along with blood vessels, we stained tissues with ionized calcium binding adaptor molecule (Iba-1) and tomato lectin respectively. Lower amount of Iba-1 expression around the coated implants compared to the control was observed (Figure 4 A and B). This presented 48% reduction ($p=0.025$) in the Iba-1 intensity than the uncoated group within 10 μm of the implant (Figure 4 C). Moreover, while the distribution pattern of blood vessels around the implants was the same in both groups (Figure 4 D and E), a significantly lower amount of lectin expression within 30 μm of electrode-tissue interface was observed in the coated implant (Figure 4 F). PDA-PSB coating yielded a 35% reduction in lectin stain intensity ($p=0.03$) compared to the uncoated group (Figure 4 F). Additionally explanted probes were stained for Iba-1 and Hoechst (Fig. S. 8). The PDA-PSB coated probed showed less attachment of microglia compared to the control probes.

3.2.5.3. Astrogliosis: GFAP antibody was used to examine reactive astrocytes around the implantation site. Fewer activated astrocytes were observed around PDA-PSB coated electrode compared to control (Figure 5, A and B). Quantitative analysis of histological data revealed that the intensity of GFAP in the coated group yielded 41% (0–10 μm; $p=0.001$), 35% (10–30 μm; $p=0.005$), 30% (30–50 μm; $p=0.025$), and 32% (50–70 μm; $p=0.011$) reduction compared to the uncoated group after one week of implantation (Figure 5 C).

3.2.5.4. Blood-brain barrier leakage: We investigated the distribution of IgG around the coated electrode compare to the uncoated group. The IgG intensity in the coated implant was lower which correlates with less glial activation around the electrode-tissue interface (Figure

Author Manuscript Author Manuscript Author Manuscript Author Manuscript

6 A and B). Quantitatively, the intensity of IgG was almost 34% ($p=0.01$) lower than the control group within 90 μm of the implantation site (Figure 6 C).

4. Discussion

In order to maintain an effective neural interface, it is necessary to minimize the undesired host tissue responses to implanted electrodes [47]. The initial tissue insult caused by electrode insertion initiates the acute inflammation by releasing of host serum proteins and activation of nearby microglia cells (~130 μm), which later can encapsulate the implant [4]. Moreover, it has been speculated that the non-specifically adsorbed protein layer on the implant surface is responsible for mediating the inflammatory cell-device interaction, which may trigger a cascade of inflammatory activation and consequently harm the performance of neural implants [4, 48]. Zwitterionic polymers exhibit high resistance to the nonspecific protein adsorption and reduce inflammatory tissue response to subcutaneous implants [17, 35]. Here, the main objective of this research was to develop a stable zwitterionic polymer coating for brain implants and to evaluate inflammatory brain tissue responses to the Zwitterionic coated implants.

4.2. Stability of the coating

The stability of the polymer film is crucial in achieving an ultra-low fouling performance in the complex biological environment [29]. While the catechol-grafted PSB showed excellent hydrophilicity and antifouling properties initially, the coating thickness decreased over 4 weeks of soaking. Since the polymer backbone is polymethacrylate, which is stable in physiological condition, the thickness reduction is most likely due to polymer falling off the surface. It is known that catechol functional groups can be oxidized to o-quinone form. The loss of catechol groups results in detachment between the PSB polymer and the substrates, with the hydrophilic polymer dissolving into the aqueous medium [49, 50].

To improve the coating stability, we developed a novel method by co-depositing PDA with PSB. *In vitro* studies showed that the polymer film (PDA-PSB) was stable over the course of a one-month period, with no significant changes in film thickness (Figure 1 C) or surface wettability (Figure 1 D) observed. PDA is known to adhere strongly to many substrates via the multiple catechol groups [51, 52]. The stability and mechanical robustness of PDA coating under physiological condition has been shown in many biomedical applications [51]. The chemical structure of PDA incorporates different functional groups like amine, catechol, and imine [39], which are amendable to covalent modification [53, 54]. Previously, zwitterionic polymers have been co-deposited with PDA to improve the antifouling properties of the PDA [55–57]. In these studies, zwitterionic polymers were pre-formed and non-covalently incorporated in PDA as dopamine polymerizes, and PDA provides the adhesion to substrates. Xu's group reported a stable PDA/PSBMA-coated propylene microfiltration membrane (PPMM) under harsh conditions, in which dopamine had directly served as both the initiator for PSBMA polymerization and the surface anchoring motif [58]. As a result, PSBMA is covalently incorporated in PDA polymer backbone. In our case, PDA is co-deposited with a catechol bearing PSB. The catechol bearing PSB polymer is capable of directly adhering to any surface via its own catechol group, but can also be physically

Author Manuscript Author Manuscript Author Manuscript Author Manuscript

entrapped in or chemically linked to the PDA (catechol of PSB participating in the dopamine polymerization) [59]. All these mechanisms could further promote coating adhesion and stability. The result in Figure 2 clearly confirms that this novel PDA-PSB co-deposition method can produce a more stable coating than PSB alone while maintaining a hydrophilic nature.

While the PDA-PSB coating is shown to be stable *in vitro* for 4 weeks, it is difficult to predict its lifetime *in vivo*. *In vivo* factors including oxidative stress in the host tissue may accelerate the polymer degradation in general [60]. Specifically, peroxidase-positive astrocytes have been shown to oxidize catechol groups, which could lead to PSB-PDA delamination [61]. Attempt to examine coating integrity was made via SEM imaging of the explanted probes after 1 week of implantation (Fig. S. 9), but it is extremely difficult to discern nm-thick organic polymer coatings from the biological materials adsorbed on the surface. The lower cell attachment on the PDA-PSB coated probes after 1 week may be an indirect evidence that the coating remained intact for at least 1 week (Fig. S. 8). Although longer term *in vivo* result is not available yet, it is possible that the antifouling coating is most valuable at the early stage of implantation when plasma protein adsorption and inflammatory cell attachments dominate the acute inflammatory response, and reduction of the early response may lead to better integration and reduced chronic response [4, 8, 62].

4.3. Anti-fouling property

To assess the anti-fouling properties of these coatings, surfaces were exposed to fibrinogen solution and fibroblast cells, respectively. There was no significant difference in protein adsorption between PSB and PDA-PSB group, while the bare Si wafer showed significantly higher protein adsorption than PSB and PDA-PSB group ($p<0.001$) (Figure 2 A). Also noted that the slightly decreased hydrophilicity of PDAPSB film resulting from incorporation of PDA doesn't affect the antifouling property of the PDA-PSB polymer film. In addition, the 3T3 fibroblast cell attachment results are consistent with protein absorption test (Figure 2 B and C). Similar performance of PSB and PDA-PSB coating were expected. Based on all *in vitro* test results, PDA-PSB showed similar anti-fouling performance to PSB but higher stability. Therefore, the PDA-PSB co-deposition method was utilized to coat electrodes tested in the *in vivo* experiments.

4.4. The effect of anti-fouling coating on brain tissue response

To maintain a stable electrode-tissue interface, the structure and surface properties of the implanted electrode must be considered [63]. Tearing of blood vessels generated by the electrode insertion causes the recruitment of macrophages derived from the bloodstream along with activated microglia to the implantation site and induces gliosis [4]. In the early stage of this process, the hydrophobic implant surface adsorbs serum proteins which may mediate the attachment and localization of inflammatory cell and consequently initiate the cascade of inflammatory responses. Additionally, many of the plasma proteins themselves such as fibrinogen, albumin, thrombin, and complement proteins are pro-inflammatory and/or neurotoxic, and can directly trigger inflammation [4]. Therefore, inhibiting protein adsorption may be useful in improving electrode biocompatibility by reducing microglial/monocyte attachment and activation upon implantation [64]. Zwitterionic coatings have been

Author Manuscript Author Manuscript Author Manuscript Author Manuscript

shown to be effective in reducing inflammatory fibrosis in subcutaneous implants, but to our knowledge, they haven't been tested on brain implants. In this paper, we characterized the cellular reactions to the PDA-PSB coated intracortical electrodes in comparison to uncoated controls after one week post-implantation in mice brain.

In our study, microglia/macrophage activity (Iba1, and lectin) was lower in the region immediately around the implanted PDA-PSB electrode compared to the control (Figure 4), which correlates well with the antifouling properties observed *in vitro*. Explant analysis showed less microglia attachment on the PDA-PSB probe's surface than the uncoated control (Fig. S. 8). This result suggests that PDA-PSB coating might suppress the recruitment and activation of microglia/macrophage by resisting nonspecific protein adsorption and cell attachment. Astroglial encapsulation occurs after the microglia activation, which is associated with a sheath consisting of activated microglia and reactive astrocytes and reduced neuronal cell density [4]. The PDA-PSB implants demonstrated reduced astrogliosis at the device-tissue interface compared to the uncoated control group (Figure 5). This effect may provide a means of improving the recorded signal quality from neural implants, because glial sheath effectively isolates the electrodes from the brain. [65] This isolation causes the degradation of signal quality that can be explained either due to increasing the distance between recording site and neuron [66] or increase in impedance [65].

The relationship between microglia and neurodegeneration has been studied in the neurodegenerative disease [67]. Similarly, at the electrode-neural tissue interface, an inverse relationship between microglia activation and neuronal cell density has been reported [13]. In this study, we investigated the axonal degeneration (NF200) along with neuronal viability (NeuN). Despite less microglia intensity around the PDA-PSB coated implants, no differences were observed between conditions for NF200 and NeuN (Figure 3). This data suggest that the initial insertion injury is the primary cause of neuronal loss at this acute stage, which should be similar in both conditions. The one-week time course is not long enough to reveal neuronal loss due to chronic inflammation around the implants. Further chronic time point studies are needed to determine the functional consequences of PDA-PSB coating on the neurodegenerative features next to the implants.

Additionally, the interactions between the microglia and the vascular system in the brain disease have been studied [68–70]. It has been shown that the activated microglia modulate the BBB integrity and function. Moreover, the vascular damage aggravates the sustained activation of microglia around the implantation site [70]. Although no differences were observed among groups for neuronal viability, significantly lower BBB leakage (IgG) was observed around the electrode in PDA-PSB coated electrodes compared to the uncoated ones, which is correlated to the microglia activation. This is an important outcome because there is a correlation between electrode functionality and BBB leakage [71] and the PDA-PSB coating may improve recording performance by reducing BBB leakage.

Different surface coating strategies for neural implants have been investigated, including electrochemical deposition of conducting polymers [72], covalent immobilization of bioactive molecules such as cell adhesion proteins and growth factors [62, 73–75], and

Author Manuscript Author Manuscript Author Manuscript Author Manuscript

incorporation of anti-inflammatory factors [76–79]. Some of these studies demonstrated the potential in modulating the inflammatory neural tissue response at the implantation site (as reviewed in [80]). However, many of the strategies explored to date have limitations. The conducting polymer coatings are limited to the tiny electrode site regions and are not sufficient to defeat the foreign body response to the entire implants. The drawbacks of protein or peptide coatings may be associated with their short half-life, being prone to enzymatic degradation [81] and the risk of immunogenicity [82, 83]. Additionally, drug-eluting coatings face the challenge of drug exhaustion after chronic implantation [80, 84]. Hydrophilic coatings that may prevent fouling have been explored as an alternative strategy (reviewed [85]), with limited success. In one study, the impact of reducing cell adhesion on the neuro-inflammatory tissue responses to electrodes was examined [64]. Parylene-C-coated glass coverslips presented significantly less activated microglial cell attachment compared to uncoated substrates in vitro, but no significant differences in inflammatory tissue responses or the density of viable neurons was observed *in vivo* [86]. Further, the conformal microgel coatings of poly(*N*-isopropylacrylamide) (pNIPAM) and acrylic acid (AAc) (pNIPAm-*co*-AAc) cross-linked with poly(ethylene glycol) (PEG) on the silicon neural electrodes was reported [87]. Although, *in vitro* analyses demonstrated significantly decreased adhesion of microglia and astrocytes in coated group compared to the uncoated control [87], the coating did not decrease the inflammatory brain tissue response at 1, 2, and 24 weeks of implant. In another study, a 4000 MW PEG coating, which showed excellent antifouling properties *in vitro* [88], did not improve the foreign body responses to neural implants [89]. On the contrary, we observed significant reductions in glial scar formation and BBB breach by our coating. These findings suggest that PSB-PDA coating effectively reduced acute inflammatory cell recruitment and activation at the interface. The difference in the results might be due to the oxidative degradation of PEG after implantation [90], superior hydrophilicity of the zwitterionc polymer coating [91], or the immunogenicity of PEG [92, 93]. Additionally, our coating is less than 3 nm thick which adds minimum change to the footprint of the device, while thicker coatings could increase the insertion damage and push the neurons away [94].

Our anti-fouling coating approach is limited to passively inhibiting all non-specific protein adsorption and cell adhesion. On the other hand, many bioactive coating strategies use bioactive molecules to promote or control a specific cellular reaction. For example, immobilizing extracellular matrix (ECM) proteins like laminin [73] and laminin-derived peptides [95, 96], or neuronal cell adhesion molecules such as L1 [62] and N-cadherin (NCad) [97] have been pursued to encourage neuronal or neurite attachment and growth on and around the neural electrodes. Alternatively, biomolecules that inhibit inflammatory cell activation such as dexamethasone [98–100], alpha-MSH [77, 101], or CD47 [102], and CD200 [103] have also been used to actively modulate inflammation. Covalently binding the L1 protein to the silicon probe surface not only promoted neuron attachment on the probe, but also inhibited microglia and astrocyte activation, and promoted neuronal survival and axonal density up to 8 weeks [62, 74]. Although these studies showed great promises in improving neural electrode biocompatibility, the stability and immunogenicity of biomolecules are still of practical concerns [82, 83], while the interactions between biomolecules with the various non-target proteins and cells *in vivo* are yet to be investigated.

Author Manuscript Author Manuscript Author Manuscript Author Manuscript

Additionally, biomolecule modification may render the surface more hydrophobic and results in higher amount of plasma protein adsorption and bacterial colonization. The best approach may be to have mosaics of biomolecules distributed at the optimum ratio on the super-hydrophilic background, so that non-specific protein and cell adhesion is inhibited, while specific cell interaction is achieved via the biomolecule domains. Such combinatorial approaches have been proposed previously, for example, the combination of PEG with a arginine-glycine-aspartic (RGD) sequence promotes fibroblast adhesion, while maintained the antifouling characteristics of the coating [104]. Also, PEG was used as a platform for the immobilization of antimicrobial peptide which reduced the bacterial adhesion along with killing the adhered bacteria to the surface [105]. Similar strategies may be used to incorporate biomolecules to the zwitterionic polymer coating to actively tune the host tissue reaction.

As discussed earlier, this study was limited to one week *in vivo* evaluation using non-functional electrode devices to mimic the implants. The result that the coating reduced the initial inflammatory host tissue response is significant in two ways. First, reducing the acute phase of inflammation in implantable biosensors intended for short term applications can improve the signal quality [106]. Secondly, studies have pointed out that controlling the initial inflammatory responses may reduce the chronic foreign body responses [4, 8, 107]. Future studies are necessary to evaluate the PDA-PSB coating for maintaining the implant functionality in the chronic time points. Moreover, since other types of cells such as oligodendrocytes, pericytes, and other infiltrating inflammatory cells are involved in the foreign body response [8, 43, 108], it is necessary to investigate the PDA-PSB coating interaction with other cells. Combining real-time imaging of the interface [7, 74] with long-term neural recording [44] may help to illustrate the dynamics of the coating mechanism. Besides surface chemistry, there are other triggers of undesired tissue responses, such as mechanical mismatch [109–111], device tethering [112–114], and device dimensions and architecture [113, 115, 116]. While the zwitterionic coating improved the acute inflammatory response, by itself, it may not be sufficient to overcome the issues mentioned above. As more advanced soft, flexible, small footprint and wireless devices are being developed to improve device-tissue integration, the anti-fouling coating can be applied on these new devices to further improve their performance.

Conclusions

In summary, we report the development of PDA-PSB co-deposition method to coat electrode surface for neural implant applications. Results demonstrated a stable and potent anti-fouling performance with the coating *in vitro*. *In vivo* evaluation revealed a significant reduction in inflammatory cell recruitment and activation, glial scar formation, and BBB breach in coated implants compared to the controls after one week, while the neuronal distribution is not affected. This finding supports future investigation aimed at using PDA-PSB coatings to enhance the duration of neural electrode functionality.

Supplementary Material

Refer to Web version on PubMed Central for supplementary material.

Author Manuscript Author Manuscript Author Manuscript Author Manuscript

Acknowledgments:

This research is financially supported by the NIH R01NS062019, R01NS089688, R21DA043817, DARPA D14AP00040 and US ArmyW81XWH-13-C-0157. The authors acknowledge the Center for Biologic Imaging (CBI) at the University of Pittsburgh for providing the imaging facility.

References:

[1]. Schwartz AB, Cui XT, Weber DJ, Moran DW, Brain-controlled interfaces: movement restoration with neural prosthetics, Neuron 52(1) (2006) 205–20. [PubMed: 17015237]

[2]. Hochberg LR, Serruya MD, Friehs GM, Mukand JA, Saleh M, Caplan AH, Branner A, Chen D, Penn RD, Donoghue JP, Neuronal ensemble control of prosthetic devices by a human with tetraplegia, Nature 442(7099) (2006) 164–71. [PubMed: 16838014]

[3]. Collinger JL, Wodlinger B, Downey JE, Wang W, Tyler-Kabara EC, Weber DJ, McMorland AJ, Velliste M, Boninger ML, Schwartz AB, High-performance neuroprosthetic control by an individual with tetraplegia, Lancet 381(9866) (2013) 557–64. [PubMed: 23253623]

[4]. Kozai TD, Jaquins-Gerstl AS, Vazquez AL, Michael AC, Cui XT, Brain tissue responses to neural implants impact signal sensitivity and intervention strategies, Acs Chem Neurosci 6(1) (2015) 48–67. [PubMed: 25546652]

[5]. Wellman SM, Eles JR, Ludwig KA, Seymour JP, Michelson NJ, McFadden WE, Vazquez AL, Kozai TDY, A Materials Roadmap to Functional Neural Interface Design, Advanced Functional Materials (2017) 1701269-n/a. [PubMed: 29805350]

[6]. Groothuis J, Ramsey NF, Ramakers GM, van der Plasse G, Physiological challenges for intracortical electrodes, Brain stimulation 7(1) (2014) 1–6. [PubMed: 23941984]

[7]. Eles JR, Vazquez AL, Kozai TDY, Cui XT, In vivo imaging of neuronal calcium during electrode implantation: Spatial and temporal mapping of damage and recovery, Biomaterials 174 (2018) 79–94. [PubMed: 29783119]

[8]. Polikov VS, Tresco PA, Reichert WM, Response of brain tissue to chronically implanted neural electrodes, J Neurosci Methods 148(1) (2005) 1–18. [PubMed: 16198003]

[9]. Anderson JM, Rodriguez A, Chang DT, FOREIGN BODY REACTION TO BIOMATERIALS, Seminars in immunology 20(2) (2008) 86–100. [PubMed: 18162407]

[10]. Kozai TD, Vazquez AL, Weaver CL, Kim SG, Cui XT, In vivo two-photon microscopy reveals immediate microglial reaction to implantation of microelectrode through extension of processes, J Neural Eng 9(6) (2012) 066001. [PubMed: 23075490]

[11]. Eles JR, Vazquez AL, Kozai TDY, Cui XT, Meningeal inflammatory response and fibrous tissue remodeling around intracortical implants: An in vivo two-photon imaging study, Biomaterials 195 (2019) 111–123. [PubMed: 30634095]

[12]. Biran R, Martin DC, Tresco PA, Neuronal cell loss accompanies the brain tissue response to chronically implanted silicon microelectrode arrays, Experimental Neurology 195(1) (2005) 115–26. [PubMed: 16045910]

[13]. McConnell GC, Rees HD, Levey AI, Gutekunst CA, Gross RE, Bellamkonda RV, Implanted neural electrodes cause chronic, local inflammation that is correlated with local neurodegeneration, J Neural Eng 6(5) (2009) 056003. [PubMed: 19700815]

[14]. Wilson CJ, Clegg RE, Leavesley DI, Pearcy MJ, Mediation of biomaterial-cell interactions by adsorbed proteins: a review, Tissue engineering 11(1–2) (2005) 1–18. [PubMed: 15738657]

[15]. Alauzun JG, Young S, D'Souza R, Liu L, Brook MA, Sheardown HD, Biocompatible, hyaluronic acid modified silicone elastomers, Biomaterials 31(13) (2010) 3471–8. [PubMed: 20138660]

[16]. Yue Z, Liu X, Molino PJ, Wallace GG, Bio-functionalisation of polydimethylsiloxane with hyaluronic acid and hyaluronic acid – Collagen conjugate for neural interfacing, Biomaterials 32(21) (2011) 4714–4724. [PubMed: 21477859]

[17]. Zhang L, Cao Z, Bai T, Carr L, Ella-Menye JR, Irvin C, Ratner BD, Jiang S, Zwitterionic hydrogels implanted in mice resist the foreign-body reaction, Nature biotechnology 31(6) (2013) 553–6.

Author Manuscript Author Manuscript Author Manuscript Author Manuscript

[18]. Rao L, Zhou H, Li T, Li C, Duan YY, Polyethylene glycol-containing polyurethane hydrogel coatings for improving the biocompatibility of neural electrodes, Acta Biomaterialia 8(6) (2012) 2233–2242. [PubMed: 22406507]

[19]. Kim DH, Wiler JA, Anderson DJ, Kipke DR, Martin DC, Conducting polymers on hydrogel-coated neural electrode provide sensitive neural recordings in auditory cortex, Acta Biomater 6(1) (2010) 57–62. [PubMed: 19651250]

[20]. Lynn AD, Kyriakides TR, Bryant SJ, Characterization of the in vitro macrophage response and in vivo host response to poly(ethylene glycol)-based hydrogels, Journal of biomedical materials research. Part A 93(3) (2010) 941–53. [PubMed: 19708075]

[21]. Muthusubramaniam L, Lowe R, Fissell WH, Li L, Marchant RE, Desai TA, Roy S, Hemocompatibility of silicon-based substrates for biomedical implant applications, Ann Biomed Eng 39(4) (2011) 1296–305. [PubMed: 21287275]

[22]. Sommakia S, Gaire J, Rickus JL, Otto KJ, Resistive and reactive changes to the impedance of intracortical microelectrodes can be mitigated with polyethylene glycol under acute in vitro and in vivo settings, Front Neuroeng 7 (2014) 33. [PubMed: 25136315]

[23]. Dalsin JL, Hu B-H, Lee BP, Messersmith PB, Mussel Adhesive Protein Mimetic Polymers for the Preparation of Nonfouling Surfaces, Journal of the American Chemical Society 125(14) (2003) 4253–4258. [PubMed: 12670247]

[24]. Browning MB, Cereceres SN, Luong PT, Cosgriff-Hernandez EM, Determination of the in vivo degradation mechanism of PEGDA hydrogels, Journal of biomedical materials research. Part A 102(12) (2014) 4244–51. [PubMed: 24464985]

[25]. Bjugstad KB, Redmond DE Jr., Lampe KJ, Kern DS, Sladek JR Jr., Mahoney MJ, Biocompatibility of PEG-based hydrogels in primate brain, Cell transplantation 17(4) (2008) 409–15. [PubMed: 18522243]

[26]. Lynn AD, Blakney AK, Kyriakides TR, Bryant SJ, Temporal progression of the host response to implanted poly(ethylene glycol)-based hydrogels, Journal of biomedical materials research. Part A 96(4) (2011) 621–31.

[27]. Cadotte AJ, DeMarse TB, Poly-HEMA as a drug delivery device for in vitro neural networks on micro-electrode arrays, Journal of Neural Engineering 2(4) (2005) 114–22. [PubMed: 16317235]

[28]. Lin C-H, Jao W-C, Yeh Y-H, Lin W-C, Yang M-C, Hemocompatibility and cytocompatibility of styrenesulfonate-grafted PDMS–polyurethane–HEMA hydrogel, Colloids and Surfaces B: Biointerfaces 70(1) (2009) 132–141. [PubMed: 19157804]

[29]. Zhao C, Li L, Wang Q, Yu Q, Zheng J, Effect of Film Thickness on the Antifouling Performance of Poly(hydroxy-functional methacrylates) Grafted Surfaces, Langmuir 27(8) (2011) 4906–4913. [PubMed: 21405141]

[30]. Campioni EG, Nobrega JN, Sefton MV, HEMA/MMMA microcapsule implants in hemiparkinsonian rat brain: biocompatibility assessment using [3H]PK11195 as a marker for gliosis, Biomaterials 19(7) (1998) 829–837. [PubMed: 9663760]

[31]. Zhang Z, Vaisocherova H, Cheng G, Yang W, Xue H, Jiang S, Nonfouling behavior of polycarboxybetaine-grafted surfaces: structural and environmental effects, Biomacromolecules 9(10) (2008) 2686–92. [PubMed: 18785772]

[32]. Zhang Z, Chen S, Chang Y, Jiang S, Surface grafted sulfobetaine polymers via atom transfer radical polymerization as superlow fouling coatings, J Phys Chem B 110(22) (2006) 10799–804. [PubMed: 16771329]

[33]. Zhang Z, Chao T, Chen S, Jiang S, Superlow fouling sulfobetaine and carboxybetaine polymers on glass slides, Langmuir 22(24) (2006) 10072–7. [PubMed: 17107002]

[34]. Jiang S, Cao Z, Ultralow-fouling, functionalizable, and hydrolyzable zwitterionic materials and their derivatives for biological applications, Adv Mater 22(9) (2010) 920–32. [PubMed: 20217815]

[35]. Ladd J, Zhang Z, Chen S, Hower JC, Jiang S, Zwitterionic polymers exhibiting high resistance to nonspecific protein adsorption from human serum and plasma, Biomacromolecules 9(5) (2008) 1357–61. [PubMed: 18376858]

[36]. Chen S, Zheng J, Li L, Jiang S, Strong Resistance of Phosphorylcholine Self-Assembled Monolayers to Protein Adsorption: Insights into Nonfouling Properties of Zwitterionic

Author Manuscript Author Manuscript Author Manuscript Author Manuscript

Materials, Journal of the American Chemical Society 127(41) (2005) 14473–14478. [PubMed: 16218643]

[37]. Chang Y, Chang W-J, Shih Y-J, Wei T-C, Hsiue G-H, Zwitterionic Sulfobetaine-Grafted Poly(vinylidene fluoride) Membrane with Highly Effective Blood Compatibility via Atmospheric Plasma-Induced Surface Copolymerization, ACS applied materials & interfaces 3(4) (2011) 1228–1237. [PubMed: 21388227]

[38]. Lee H, Lee Y, Statz AR, Rho J, Park TG, Messersmith PB, Substrate-Independent Layer-by-Layer Assembly by Using Mussel-Adhesive-Inspired Polymers, Advanced Materials 20(9) (2008) 1619–1623. [PubMed: 22228925]

[39]. Lee H, Dellatore SM, Miller WM, Messersmith PB, Mussel-inspired surface chemistry for multifunctional coatings, Science 318(5849) (2007) 426–30. [PubMed: 17947576]

[40]. Li G, Cheng G, Xue H, Chen S, Zhang F, Jiang S, Ultra low fouling zwitterionic polymers with a biomimetic adhesive group, Biomaterials 29(35) (2008) 4592–7. [PubMed: 18819708]

[41]. Gao C, Li G, Xue H, Yang W, Zhang F, Jiang S, Functionalizable and ultra-low fouling zwitterionic surfaces via adhesive mussel mimetic linkages, Biomaterials 31(7) (2010) 1486–92. [PubMed: 19962753]

[42]. Sundaram HS, Han X, Nowinski AK, Ella-Menye JR, Wimbish C, Marek P, Senecal K, Jiang S, One-step dip coating of zwitterionic sulfobetaine polymers on hydrophobic and hydrophilic surfaces, ACS applied materials & interfaces 6(9) (2014) 6664–71. [PubMed: 24730392]

[43]. Kozai TD, Gugel Z, Li X, Gilgunn PJ, Khilwani R, Ozdoganlar OB, Fedder GK, Weber DJ, Cui XT, Chronic tissue response to carboxymethyl cellulose based dissolvable insertion needle for ultra-small neural probes, Biomaterials 35(34) (2014) 9255–68. [PubMed: 25128375]

[44]. Golabchi A, Wu B, Li X, Carlisle DL, Kozai TDY, Friedlander RM, Cui XT, Melatonin improves quality and longevity of chronic neural recording, Biomaterials 180 (2018) 225–239. [PubMed: 30053658]

[45]. Hassel B.r., Iversen EG, Fonnum F, Neurotoxicity of albumin in vivo, Neuroscience Letters 167(1) (1994) 29–32. [PubMed: 7909931]

[46]. Winslow BD, Tresco PA, Quantitative analysis of the tissue response to chronically implanted microwire electrodes in rat cortex, Biomaterials 31(7) (2010) 1558–67. [PubMed: 19963267]

[47]. Aregueta-Robles UA, Woolley AJ, Poole-Warren LA, Lovell NH, Green RA, Organic electrode coatings for next-generation neural interfaces, Front Neuroeng 7 (2014) 15. [PubMed: 24904405]

[48]. Fattahi P, Yang G, Kim G, Abidian MR, A review of organic and inorganic biomaterials for neural interfaces, Adv Mater 26(12) (2014) 1846–85. [PubMed: 24677434]

[49]. Balla J, Kiss T, Jameson RF, Copper(II)-catalyzed oxidation of catechol by molecular oxygen in aqueous solution, Inorganic Chemistry 31(1) (1992) 58–62.

[50]. Utzig T, Stock P, Valtiner M, Resolving Non-Specific and Specific Adhesive Interactions of Catechols at Solid/Liquid Interfaces at the Molecular Scale, Angew Chem Int Ed Engl 55(33) (2016) 9524–8. [PubMed: 27374053]

[51]. Ding YH, Floren M, Tan W, Mussel-inspired polydopamine for bio-surface functionalization, Biosurface and Biotribology 2(4) (2016) 121–136. [PubMed: 29888337]

[52]. Barclay T, Hegab HM, Clarke S, Ginic-Markovic M, Versatile Surface Modification Using Polydopamine and Related Polycatecholamines: Chemistry, Structure, and Applications, 2017.

[53]. Zhai L, Cebeci FÇ, Cohen RE, Rubner MF, Stable Superhydrophobic Coatings from Polyelectrolyte Multilayers, Nano Letters 4(7) (2004) 1349–1353.

[54]. Kim HS, Ham HO, Son YJ, Messersmith PB, Yoo HS, Electrospun catechol-modified poly(ethyleneglycol) nanofibrous mesh for anti-fouling properties, Journal of Materials Chemistry B 1(32) (2013) 3940–3949.

[55]. Chang C-C, Kolewe KW, Li Y, Kosif I, Freeman BD, Carter KR, Schiffman JD, Emrick T, Underwater Superoleophobic Surfaces Prepared from Polymer Zwitterion/Dopamine Composite Coatings, Advanced Materials Interfaces 3(6) (2016) 1500521. [PubMed: 27774375]

[56]. Zhou R, Ren P-F, Yang H-C, Xu Z-K, Fabrication of antifouling membrane surface by poly(sulfobetaine methacrylate)/polydopamine co-deposition, Journal of Membrane Science 466 (2014) 18–25.

Author Manuscript Author Manuscript Author Manuscript Author Manuscript

[57]. Kolewe KW, Dobosz KM, Rieger KA, Chang C-C, Emrick T, Schiffman JD, Antifouling Electrospun Nanofiber Mats Functionalized with Polymer Zwitterions, ACS applied materials & interfaces 8(41) (2016) 27585–27593. [PubMed: 27669057]

[58]. Zhang C, Ma M-Q, Chen T-T, Zhang H, Hu D-F, Wu B-H, Ji J, Xu Z-K, Dopamine-Triggered One-Step Polymerization and Codeposition of Acrylate Monomers for Functional Coatings, ACS applied materials & interfaces 9(39) (2017) 34356–34366. [PubMed: 28893062]

[59]. Wang L, Xu H, Song Y, Luo J, Wei W, Xu S, Cai X, Highly sensitive detection of quantal dopamine secretion from pheochromocytoma cells using neural microelectrode array electrodeposited with polypyrrole graphene, ACS applied materials & interfaces 7(14) (2015) 7619–26. [PubMed: 25804204]

[60]. Takmakov P, Ruda K, Scott Phillips K, Isayeva IS, Krauthamer V, Welle CG, Rapid evaluation of the durability of cortical neural implants using accelerated aging with reactive oxygen species, J Neural Eng 12(2) (2015) 026003. [PubMed: 25627426]

[61]. Schipper HM, Kotake Y, Janzen EG, Catechol oxidation by peroxidase-positive astrocytes in primary culture: an electron spin resonance study, The Journal of Neuroscience 11(7) (1991) 2170–2176. [PubMed: 1712380]

[62]. Azemi E, Lagenaur CF, Cui XT, The surface immobilization of the neural adhesion molecule L1 on neural probes and its effect on neuronal density and gliosis at the probe/tissue interface, Biomaterials 32(3) (2011) 681–92. [PubMed: 20933270]

[63]. Stieglitz T, Considerations on surface and structural biocompatibility as prerequisite for long-term stability of neural prostheses, Journal of nanoscience and nanotechnology 4(5) (2004) 496–503. [PubMed: 15503435]

[64]. Leung BK, Biran R, Underwood CJ, Tresco PA, Characterization of microglial attachment and cytokine release on biomaterials of differing surface chemistry, Biomaterials 29(23) (2008) 3289–97. [PubMed: 18485471]

[65]. Turner JN, Shain W, Szarowski DH, Andersen M, Martins S, Isaacson M, Craighead H, Cerebral astrocyte response to micromachined silicon implants, Exp Neurol 156(1) (1999) 33–49. [PubMed: 10192775]

[66]. Xindong L, B. MD, R. CR, A. BL, H. YTG, F. AW, Stability of the interface between neural tissue and chronically implanted intracortical microelectrodes, IEEE Transactions on Rehabilitation Engineering 7(3) (1999) 315–326. [PubMed: 10498377]

[67]. Block ML, Zecca L, Hong JS, Microglia-mediated neurotoxicity: uncovering the molecular mechanisms, Nat Rev Neurosci 8(1) (2007) 57–69. [PubMed: 17180163]

[68]. da Fonseca ACC, Matias D, Garcia C, Amaral R, Geraldo LH, Freitas C, Lima FRS, The impact of microglial activation on blood-brain barrier in brain diseases, Frontiers in Cellular Neuroscience 8 (2014) 362. [PubMed: 25404894]

[69]. Bowyer JF, Sarkar S, Tranter KM, Hanig JP, Miller DB, O'Callaghan JP, Vascular-directed responses of microglia produced by methamphetamine exposure: indirect evidence that microglia are involved in vascular repair?, Journal of neuroinflammation 13(1) (2016) 64. [PubMed: 26970737]

[70]. Thurgur H, Pinteaux E, Microglia in the Neurovascular Unit: Blood–Brain Barrier–microglia Interactions After Central Nervous System Disorders, Neuroscience (2018).

[71]. Saxena T, Karumbaiah L, Gaupp EA, Patkar R, Patil K, Betancur M, Stanley GB, Bellamkonda RV, The impact of chronic blood-brain barrier breach on intracortical electrode function, Biomaterials 34(20) (2013) 4703–13. [PubMed: 23562053]

[72]. Cui X, Martin DC, Electrochemical deposition and characterization of poly(3,4-ethylenedioxythiophene) on neural microelectrode arrays, Sensors and Actuators B: Chemical 89(1) (2003) 92–102.

[73]. He W, McConnell GC, Bellamkonda RV, Nanoscale laminin coating modulates cortical scarring response around implanted silicon microelectrode arrays, J Neural Eng 3(4) (2006) 316–26. [PubMed: 17124336]

[74]. Eles JR, Vazquez AL, Snyder NR, Lagenaur C, Murphy MC, Kozai TD, Cui XT, Neuroadhesive L1 coating attenuates acute microglial attachment to neural electrodes as revealed by live two-photon microscopy, Biomaterials 113 (2017) 279–292. [PubMed: 27837661]

Author Manuscript Author Manuscript Author Manuscript Author Manuscript

[75]. Kolarcik CL, Bourbeau D, Azemi E, Rost E, Zhang L, Lagenaur CF, Weber DJ, Cui XT, In vivo effects of L1 coating on inflammation and neuronal health at the electrode–tissue interface in rat spinal cord and dorsal root ganglion, Acta Biomaterialia 8(10) (2012) 3561–3575. [PubMed: 22750248]

[76]. Potter KA, Jorfi M, Householder KT, Foster EJ, Weder C, Capadona JR, Curcumin-releasing mechanically adaptive intracortical implants improve the proximal neuronal density and blood-brain barrier stability, Acta Biomater 10(5) (2014) 2209–22. [PubMed: 24468582]

[77]. Zhong Y, Bellamkonda RV, Controlled release of anti-inflammatory agent alpha-MSH from neural implants, Journal of controlled release : official journal of the Controlled Release Society 106(3) (2005) 309–18. [PubMed: 15978692]

[78]. Kozai TDY, Jaquins-Gerstl AS, Vazquez AL, Michael AC, Cui XT, Dexamethasone retrodialysis attenuates microglial response to implanted probes in vivo, Biomaterials 87 (2016) 157–169. [PubMed: 26923363]

[79]. Gomez N, Lu Y, Chen S, Schmidt CE, Immobilized nerve growth factor and microtopography have distinct effects on polarization versus axon elongation in hippocampal cells in culture, Biomaterials 28(2) (2007) 271–84. [PubMed: 16919328]

[80]. Woeppel K, Yang Q, Cui XT, Recent advances in neural electrode–tissue interfaces, Current Opinion in Biomedical Engineering 4(Supplement C) (2017) 21–31. [PubMed: 29423457]

[81]. Raza F, Zafar H, Zhu Y, Ren Y, Ullah A, Khan AU, He X, Han H, Aquib M, Boakye-Yiadom KO, Ge L, A Review on Recent Advances in Stabilizing Peptides/Proteins upon Fabrication in Hydrogels from Biodegradable Polymers, Pharmaceutics 10(1) (2018).

[82]. Galili U, Avoiding detrimental human immune response against Mammalian extracellular matrix implants, Tissue engineering. Part B, Reviews 21(2) (2015) 231–41. [PubMed: 25315097]

[83]. Ratner B, Hoffman A, Schoen F, Lwemons J, Biomaterials Science: An Introduction to Materials in Medicine, ACADEMIC PRESS 2004.

[84]. Luo S-C, Sekine J, Zhu B, Zhao H, Nakao A, Yu H.-h., Polydioxythiophene Nanodots, Nonowires, Nano-Networks, and Tubular Structures: The Effect of Functional Groups and Temperature in Template-Free Electropolymerization, ACS Nano 6(4) (2012) 3018–3026. [PubMed: 22424318]

[85]. Vaisocherová H, Brynda E, Homola J, Functionalizable low-fouling coatings for label-free biosensing in complex biological media: advances and applications, Analytical and Bioanalytical Chemistry 407(14) (2015) 3927–3953. [PubMed: 25821150]

[86]. Winslow BD, Christensen MB, Yang WK, Solzbacher F, Tresco PA, A comparison of the tissue response to chronically implanted Parylene-C-coated and uncoated planar silicon microelectrode arrays in rat cortex, Biomaterials 31(35) (2010) 9163–72. [PubMed: 20561678]

[87]. Gutowski SM, Templeman KL, South AB, Gaulding JC, Shoemaker JT, LaPlaca MC, Bellamkonda RV, Lyon LA, García AJ, Host response to microgel coatings on neural electrodes implanted in the brain, Journal of biomedical materials research. Part A 102(5) (2014) 1486–1499. [PubMed: 23666919]

[88]. Su Y-L, Cheng W, Li C, Jiang Z, Preparation of antifouling ultrafiltration membranes with poly(ethylene glycol)-graft-polyacrylonitrile copolymers, Journal of Membrane Science 329(1) (2009) 246–252.

[89]. Lee HC, Gaire J, Currlin SW, McDermott MD, Park K, Otto KJ, Foreign Body Response to Intracortical Microelectrodes Is Not Altered with Dip-Coating of Polyethylene Glycol (PEG), Frontiers in neuroscience 11 (2017) 513–513. [PubMed: 28959183]

[90]. Ulbricht J, Jordan R, Luxenhofer R, On the biodegradability of polyethylene glycol, polypeptoids and poly(2-oxazoline)s, Biomaterials 35(17) (2014) 4848–61. [PubMed: 24651032]

[91]. Chen J-S, Ting Y-S, Tsou H-M, Liu T-Y, Highly hydrophilic and antibiofouling surface of zwitterionic polymer immobilized on polydimethylsiloxane by initiator-free atmospheric plasma-induced polymerization, Surface and Coatings Technology 344 (2018) 621–625.

[92]. Schellekens H, Hennink WE, Brinks V, The immunogenicity of polyethylene glycol: facts and fiction, Pharmaceutical research 30(7) (2013) 1729–34. [PubMed: 23673554]

Author Manuscript Author Manuscript Author Manuscript Author Manuscript

[93]. Yang Q, Lai SK, Anti-PEG immunity: emergence, characteristics, and unaddressed questions, Wiley interdisciplinary reviews. Nanomedicine and nanobiotechnology 7(5) (2015) 655–677. [PubMed: 25707913]

[94]. Singh S, Lo M-C, Damodaran VB, Kaplan HM, Kohn J, Zahn JD, Shreiber DI, Modeling the Insertion Mechanics of Flexible Neural Probes Coated with Sacrificial Polymers for Optimizing Probe Design, Sensors (Basel, Switzerland) 16(3) (2016) 330.

[95]. Righi M, Puleo GL, Tonazzini I, Giudetti G, Cecchini M, Micera S, Peptide-based coatings for flexible implantable neural interfaces, Scientific reports 8(1) (2018) 502. [PubMed: 29323135]

[96]. Cui X, Wiler J, Dzaman M, Altschuler RA, Martin DC, In vivo studies of polypyrrole/peptide coated neural probes, Biomaterials 24(5) (2003) 777–787. [PubMed: 12485796]

[97]. Collazos-Castro JE, Hernández-Labrado GR, Polo JL, García-Rama C, N-Cadherin- and L1-functionalised conducting polymers for synergistic stimulation and guidance of neural cell growth, Biomaterials 34(14) (2013) 3603–3617. [PubMed: 23422593]

[98]. Kolarcik CL, Catt K, Rost E, Albrecht IN, Bourbeau D, Du Z, Kozai TD, Luo X, Weber DJ, Cui XT, Evaluation of poly(3,4-ethylenedioxythiophene)/carbon nanotube neural electrode coatings for stimulation in the dorsal root ganglion, J Neural Eng 12(1) (2015) 016008. [PubMed: 25485675]

[99]. Spataro L, Dilgen J, Retterer S, Spence AJ, Isaacson M, Turner JN, Shain W, Dexamethasone treatment reduces astroglia responses to inserted neuroprosthetic devices in rat neocortex, Exp Neurol 194(2) (2005) 289–300. [PubMed: 16022859]

[100]. Zhong Y, Bellamkonda RV, Dexamethasone-coated neural probes elicit attenuated inflammatory response and neuronal loss compared to uncoated neural probes, Brain Research 1148(0) (2007) 15–27. [PubMed: 17376408]

[101]. He W, McConnell GC, Schneider TM, Bellamkonda RV, A novel anti-inflammatory surface for neural electrodes, Advanced Materials 19(21) (2007) 3529-+.

[102]. Tengood JE, Levy RJ, Stachelek SJ, The use of CD47-modified biomaterials to mitigate the immune response, Experimental biology and medicine 241(10) (2016) 1033–41. [PubMed: 27190273]

[103]. Chen EY, Chu S-H, Gov L, Kim YK, Lodoen MB, Tenner AJ, Liu WF, CD200 modulates macrophage cytokine secretion and phagocytosis in response to poly(lactic-co-glycolic acid) microparticles and films, Journal of Materials Chemistry B 5(8) (2017) 1574–1584. [PubMed: 28736613]

[104]. Satomi T, Nagasaki Y, Kobayashi H, Otsuka H, Kataoka K, Density control of poly(ethylene glycol) layer to regulate cellular attachment, Langmuir 23(12) (2007) 6698–703. [PubMed: 17480105]

[105]. Palomero JB, Development of polymeric coatings with combined antifouling/antibacterial properties for titanium dental implants, Technical University of Catalonia, 2017.

[106]. Xie X, Doloff JC, Yesilyurt V, Sadraei A, McGarrigle JJ, Omami M, Veiseh O, Farah S, Isa D, Ghani S, Joshi I, Vegas A, Li J, Wang W, Bader A, Tam HH, Tao J, Chen H.-j., Yang B, Williamson KA, Oberholzer J, Langer R, Anderson DG, Reduction of measurement noise in a continuous glucose monitor by coating the sensor with a zwitterionic polymer, Nature Biomedical Engineering 2(12) (2018) 894–906.

[107]. Rennaker RL, Miller J, Tang H, Wilson DA, Minocycline increases quality and longevity of chronic neural recordings, J Neural Eng 4(2) (2007) L1–5. [PubMed: 17409469]

[108]. Wellman SM, Cambi F, Kozai TD, The role of oligodendrocytes and their progenitors on neural interface technology: A novel perspective on tissue regeneration and repair, Biomaterials 183 (2018) 200–217. [PubMed: 30172245]

[109]. Goldstein SR, Salcman M, Mechanical factors in the design of chronic recording intracortical microelectrodes, IEEE Trans Biomed Eng 20(4) (1973) 260–9. [PubMed: 4196687]

[110]. Edell DJ, Toi VV, McNeil VM, Clark LD, Factors influencing the biocompatibility of insertable silicon microshafts in cerebral cortex, IEEE Trans Biomed Eng 39(6) (1992) 635–43. [PubMed: 1601445]

Author Manuscript Author Manuscript Author Manuscript Author Manuscript

[111]. Sharp AA, Ortega AM, Restrepo D, Curran-Everett D, Gall K, In vivo penetration mechanics and mechanical properties of mouse brain tissue at micrometer scales, IEEE Trans Biomed Eng 56(1) (2009) 45–53. [PubMed: 19224718]

[112]. Biran R, Martin DC, Tresco PA, The brain tissue response to implanted silicon microelectrode arrays is increased when the device is tethered to the skull, Journal of biomedical materials research. Part A 82(1) (2007) 169–78. [PubMed: 17266019]

[113]. Thelin J, Jorntell H, Psouni E, Garwicz M, Schouenborg J, Danielsen N, Linsmeier CE, Implant size and fixation mode strongly influence tissue reactions in the CNS, PLoS One 6(1) (2011) e16267. [PubMed: 21298109]

[114]. Kim YT, Hitchcock RW, Bridge MJ, Tresco PA, Chronic response of adult rat brain tissue to implants anchored to the skull, Biomaterials 25(12) (2004) 2229–37. [PubMed: 14741588]

[115]. Stice P, Gilletti A, Panitch A, Muthuswamy J, Thin microelectrodes reduce GFAP expression in the implant site in rodent somatosensory cortex, J Neural Eng 4(2) (2007) 42–53. [PubMed: 17409479]

[116]. Seymour JP, Kipke DR, Neural probe design for reduced tissue encapsulation in CNS, Biomaterials 28(25) (2007) 3594–607. [PubMed: 17517431]

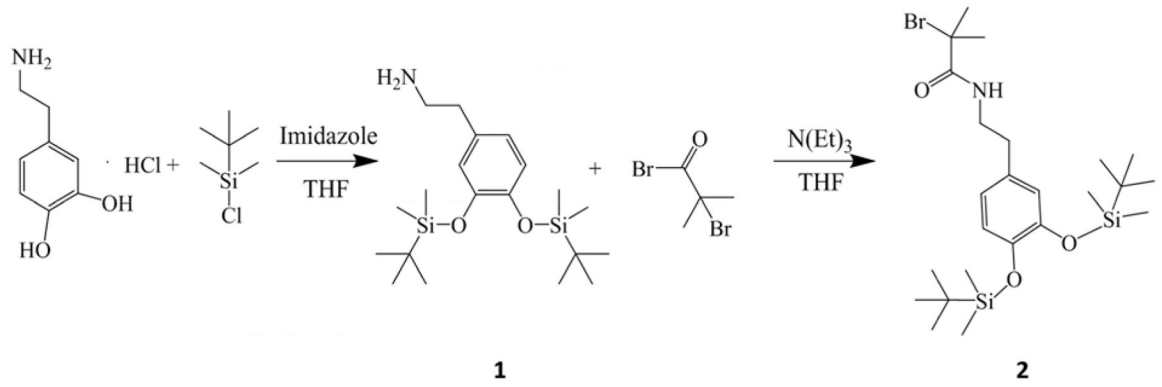

Scheme 1.
Reaction steps to synthesis the catechol initiator with hydroxyl protection.

Author Manuscript Author Manuscript Author Manuscript Author Manuscript

Author Manuscript Author Manuscript Author Manuscript Author Manuscript

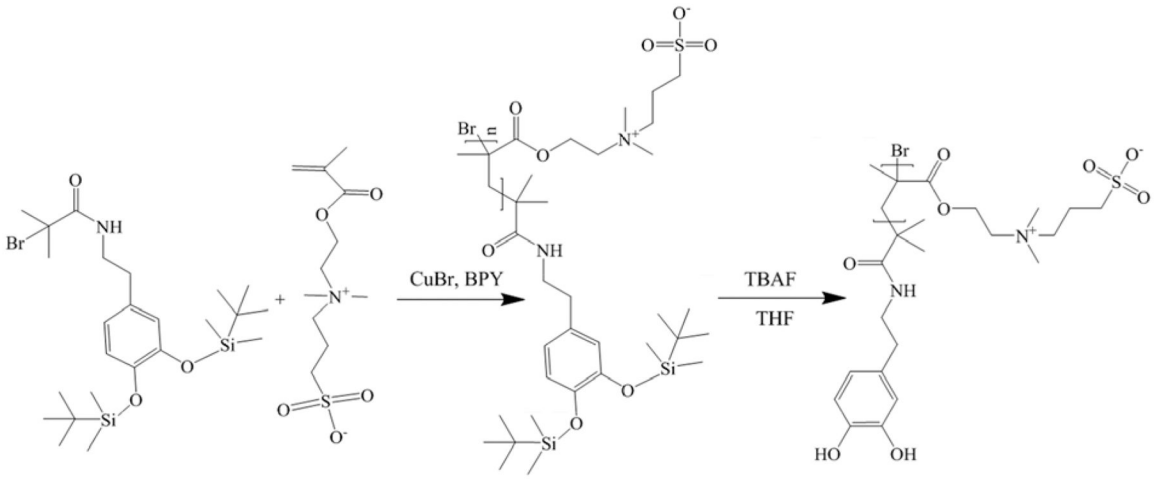

Scheme 2.

Reaction steps for grafting PSB through catechol initiator via ATRP, and de-protection of hydroxyl group before surface adhesion.

Author Manuscript Author Manuscript Author Manuscript Author Manuscript

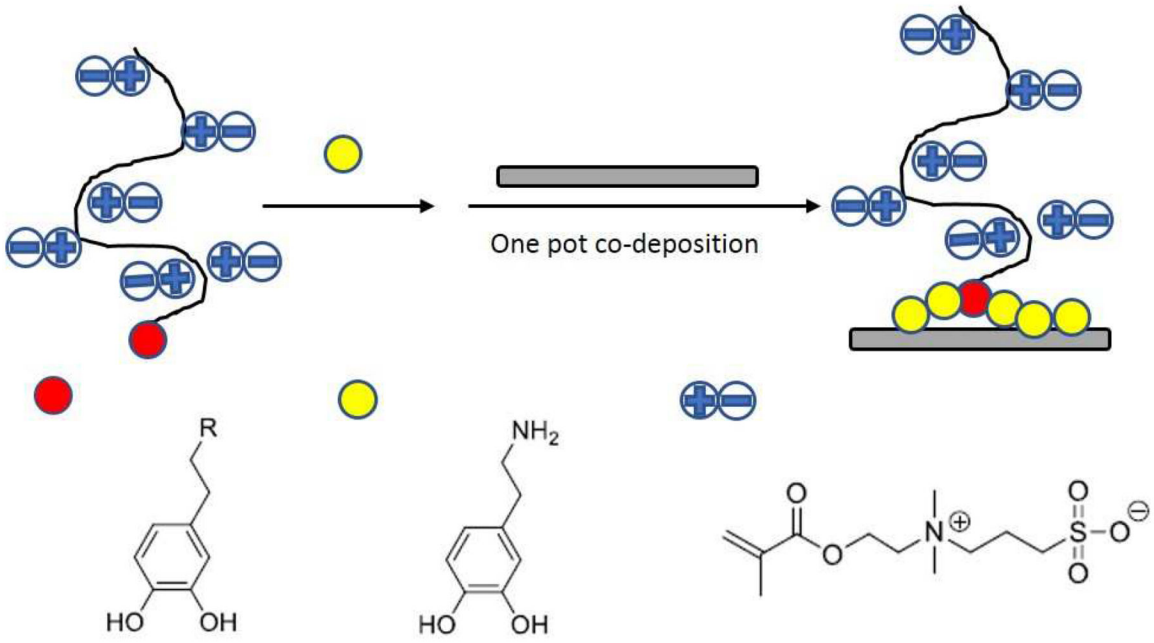

Scheme 3.
Schematic demonstration of PDA-PSB co-deposition surface coating method.

Author Manuscript Author Manuscript Author Manuscript Author Manuscript

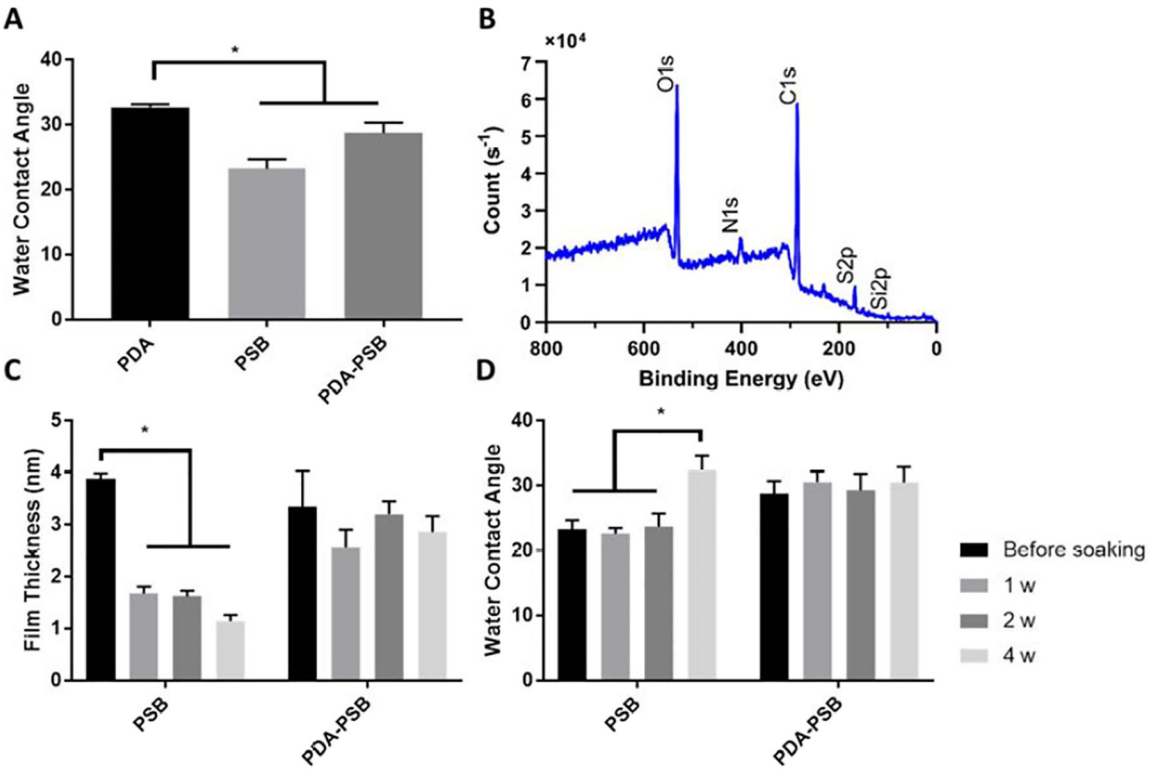

Figure 1.

Surface characterization of the coating. (A) Water contact angle of PDA, PSB, and PDA-PSD polymer film before soaking in PBS. (B) XPS spectra of PDA-PSB film coated on a Si wafer. Each peak is labeled with corresponding elements. (C) Polymer film thickness changes of PSB and PDA-PSB before and after soaking in PSB up to 4 weeks. N=8 before soaking and 1 w and N=6 at 2 w and 4 w in both PSB and PDA-PSB groups. (D) Polymer film water contact angle changes of PSB and PDA-PSB before and after soaking in PBS up to 4 weeks. Before soaking and 1 w N= 6 PSB, and N=4 PDA-PSB; at 2 w and 4 w N=6 for PSB and PDA-PSB groups. Data showed as mean ±SE; * indicates $p<0.05$. The relatively smaller portion of PDA incorporation significantly enhanced the polymer stability for at least 4 weeks *in vitro*.

Author Manuscript Author Manuscript Author Manuscript Author Manuscript

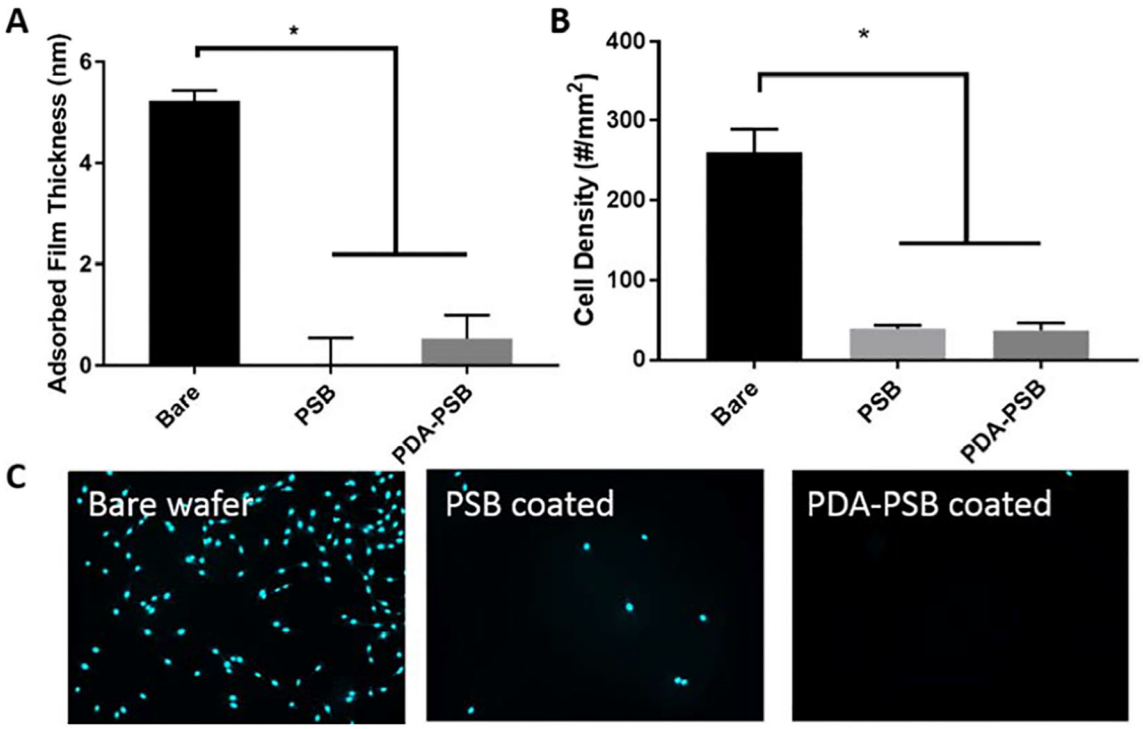

Figure 2.

PSB coating resists protein adsorption and cell adhesion (A) Protein adsorption comparison between bare, PSB, and PDA-PSB coated wafer. (B and C) 3T3 fibroblast cell attachment assay results for bare, PSB coated, and PDA-PSB coated wafer. Cyan (nuclei). For section A, N= 4 and for section B, N=8 for Bare, PSB and PDA-PSB groups. Data showed as mean ±SE; * indicates $p<0.05$.

Author Manuscript Author Manuscript Author Manuscript Author Manuscript

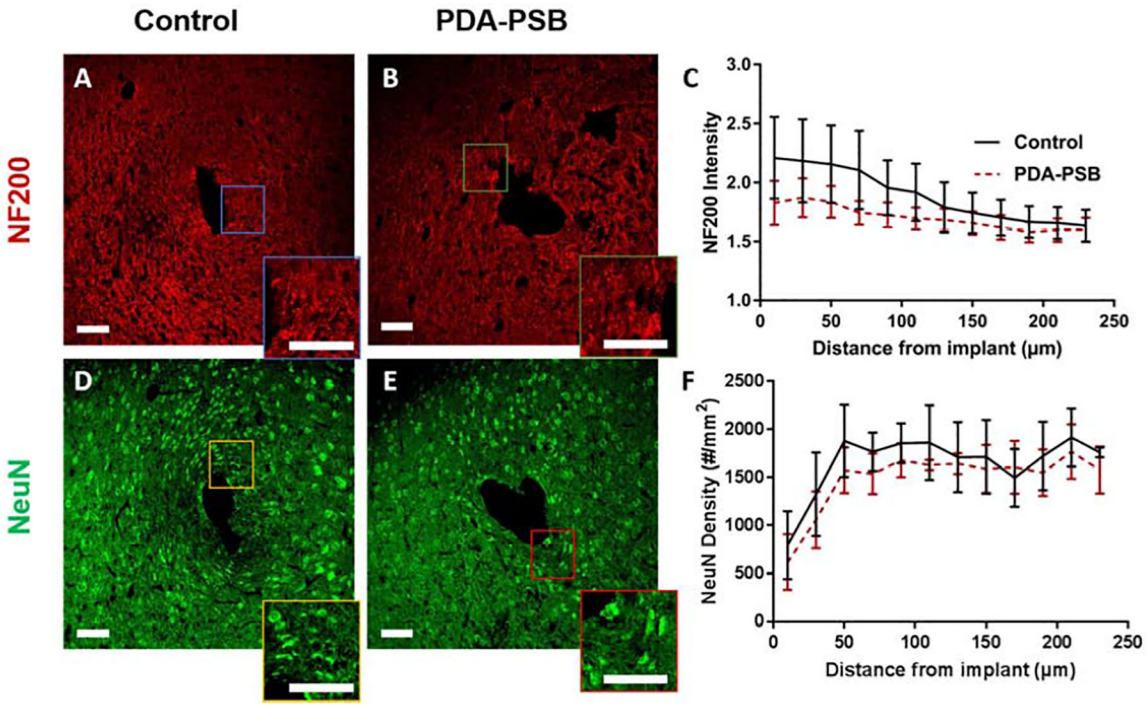

Figure 3.

Representative immunofluorescence images of NF200 (red, neurofilament; A and B) and NeuN (green, neuronal cell, D and E) around single shank electrode in control (A and D) and PDA-PSB (B and E) groups. Inset showing higher magnification images. All scale bars are 100 μm. (C) is the normalized intensity values for NF200 expression (histological samples, for control N=4. animal, N=8 sample; PDAPSB N=4 animal, N=8 sample). (F) Cell density counts per mm^2 of neuronal cells at 1 week post-implant are presented (histological samples, for control N=4. animal, N=5 sample; PDA-PSB N=4 animal, N=9 sample). Results were binned 10 μm from the electrode-tissue interface until 240 μm away, with 20 μm bin size. Data showed as mean ±SE. * indicates $p<0.05$.

Author Manuscript Author Manuscript Author Manuscript Author Manuscript

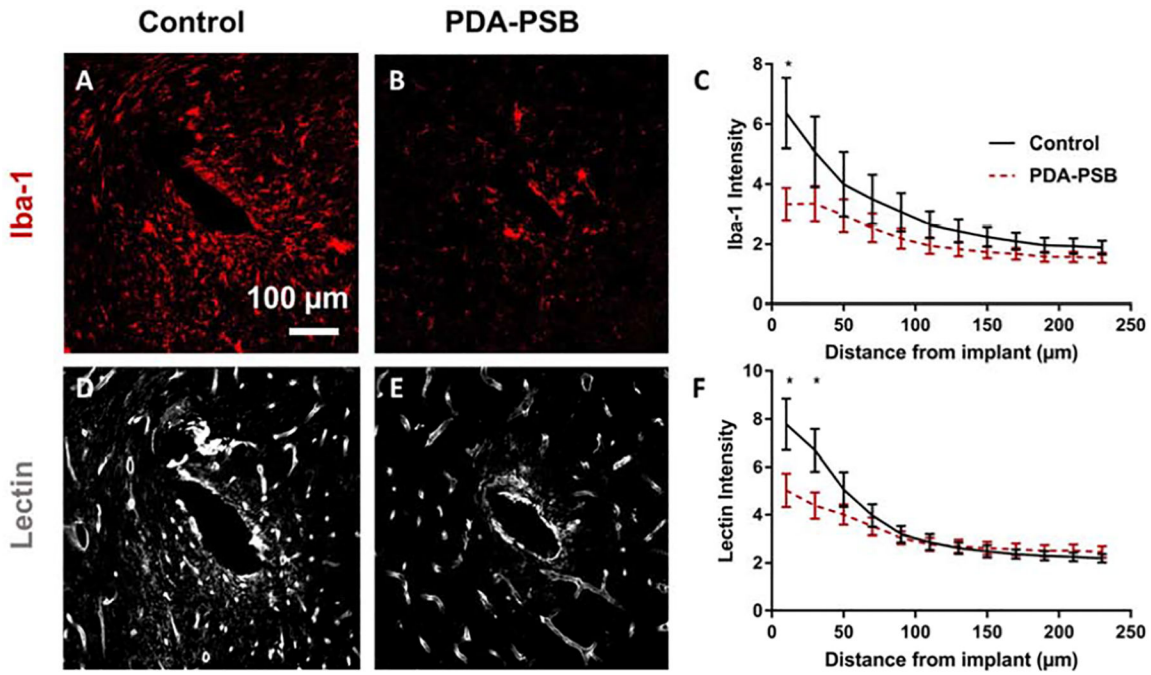

Figure 4.

Representative image of Iba-1 and Lectin staining for reactive microglia and vascular endothelium 1 week post-implantation in uncoated (A and D) and PDA-PSB coated (B and E) probes. Scale bar=100 μm. (C and F) are the normalized intensity value for Iba-1 expression (histological samples, for control N=4. animal, N=8 sample; PDA-PSB N=4 animal, N=8 sample), and lectin (histological samples, for control N=4 animal, N=18 sample; PDA-PSB N=4 animal, N=18 sample) as a function of distance from implant 1 week after implantation. Intensities were calculated 10 μm from the implant site until 240 μm away, with 20 μm bin size. Data presented as mean ±SE; * indicates $p<0.05$.

Author Manuscript Author Manuscript Author Manuscript Author Manuscript

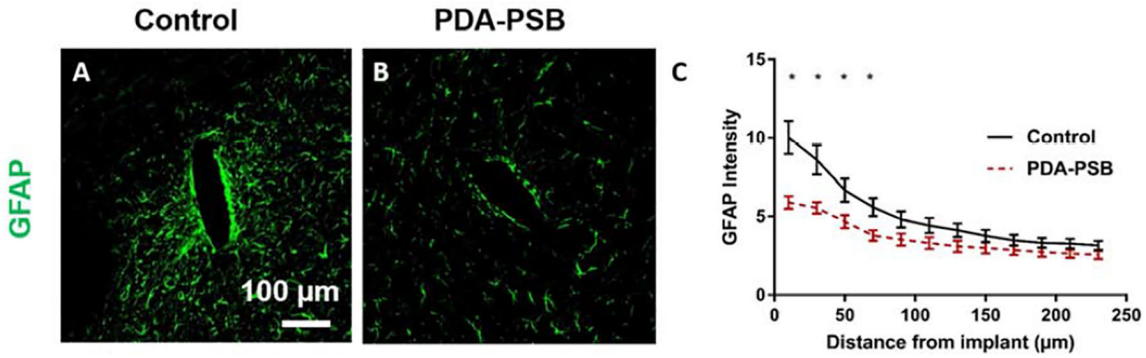

Figure 5.

Representative images of GFAP staining for reactive astrocytes 1 week post-implantation in uncoated (A) and PDA-PSB (B) coated probes. Scale bar=100 µm. (C) GFAP fluorescent intensity profiles as a function of distance from implant 1 week after implantation (histological samples, for control N=4 animal, N=18 sample; PDA-PSB N=4 animal, N=18 sample). Intensities were calculated 10 µm from the implant site until 240 µm away, with 20 µm bin size. Data presented as mean ±SE; * indicates $p<0.05$.

Author Manuscript Author Manuscript Author Manuscript Author Manuscript

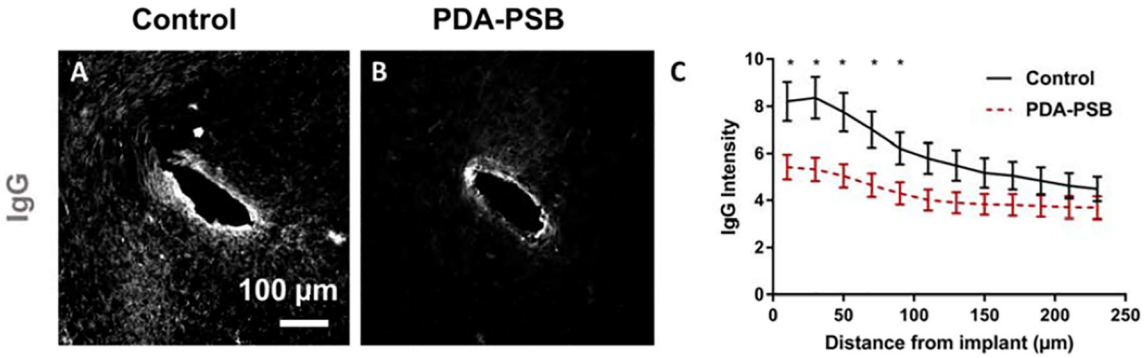

Figure 6.

Immunohistochemical IgG staining (marker of BBB leakage; A and B) around single shank electrode in control (A) and PDA-PSB (B) groups. Scale bar in A and B is 100 µm. (C) is the normalized intensity values for IgG expression (histological samples, for control N=4. animal, N=8 sample; PDA-PSB N=4 animal, N=8 sample. Results were binned 10 µm from the electrode-tissue interface until 240 µm away, with 20 µm bin size. Data showed as mean ±SE; * indicates $p<0.05$.